Wavelength dependent propagation and reconstruction of white light Bessel beams

P Fischer[1]**, H Little**[1]**, R L Smith**[2]**, C Lopez-Mariscal**[1,3]**,
C T A Brown**[1]**, W Sibbett**[1] **and K Dholakia**[1]

[1] SUPA, J F Allen Research Labs, School of Physics and Astronomy, University of
St Andrews, Fife, KY16 9SS, UK
[2] Illnois Wesleyan University, PO Box 2900, Bloomington, IL 61702-2900, USA
[3] Photonics and Mathematical Optics Group, Tecnologico de Monterrey, 64849, Mexico

E-mail: fischer@phadreus.ch

Abstract
Bessel beams are propagation invariant light fields. It has very recently been
shown that they may be created with temporally incoherent (white) light.
Such fields may have applications in low coherence interferometric imaging
for biomedicine and optical micromanipulation. White light Bessel beams
may be deemed at first glance to generate a white focal line of light at the
beam centre due to the absence of chromatic aberration. We investigate the
spectral characteristics of the reformation or self-healing of this light field in
the presence of a circular obstruction and reveal that the spectral
characteristics of the beam generation and reformation results in a dispersive
focal line at the beam centre which is 'white' only over a certain region.

Keywords: white light Bessel beams, reconstruction, dispersion

(Some figures in this article are in colour only in the electronic version)

1. Introduction

Optically sculpted light fields have found significant application in a wide variety of fields including studies of optical angular momentum, atomic and particle micromanipulation, nonlinear optics and quantum communication [1–6]. They have also enabled new studies in colloidal dynamics and the optical separation of microscopic objects. Such 'sculpted' light fields do not typically possess the standard irradiance or phase variations one associates with TEM_{00} Gaussian beams but may have unusual irradiance profiles combined with non-planar wavefronts. Examples include Laguerre–Gaussian and Bessel light beams. These latter fields are solutions to the Helmholtz equation that are propagation invariant or 'pseudo-non diffracting', originally explored by Durnin and co-workers [1, 7]. The monochromatic zero-order Bessel beam has a narrow central region surrounded by a series of concentric rings with higher order forms of this beam possessing an orbital angular momentum optical vortex on axis. The wavevector of the Bessel beam has a radial and axial component. Overall, the Bessel beam may be considered as consisting of an overlap of conical wavevectors. The conical nature of the wavevectors leads to an important property of self-healing or reconstruction where the beam may reform beyond an obstacle. This property has been used for micromanipulation in multiple planes [3]. Very recently, the first white light Bessel beam was demonstrated and the influence of temporal and spatial coherence on the resulting beam pattern was discussed [8, 9].

The Bessel beam has its power distributed equally between its rings [10]. An increased number of rings lead to an extended distance of propagation invariant behaviour but at the expense of power in the central maximum. Durnin *et al* [1] showed that by detailed consideration optimized Gaussian and Bessel beams are comparably efficient at transporting power. Ultimately one is trading power for enhanced depth of focus in this system.

The Bessel light field may be deemed as a set of propagating wavevectors on a cone, as stated, and this leads to the intriguing property of self-healing. Placing an opaque obstruction in the centre of the beam would normally mean we are blocking the light and it is just diffraction that would allow some light to re-appear on the beam axis. For the Bessel

light field however, the conical waves that constitute the centre of the beam are able to move past the obstruction, casting a shadow into the beam, but ultimately reforming some distance beyond the object with the characteristic Bessel beam intensity transverse profile. For an opaque object, we can denote the distance after which the beam reforms using simple geometric arguments relating the radial and overall wavevectors of the light field. Reconstruction of monochromatic Bessel beams has been seen and indeed used for optical micromanipulation [3]. Reformation of a Bessel beam created by thermal light sources has recently been observed [9] but importantly not analysed to any extent.

In this paper, we investigate the reconstruction of white light Bessel beams in detail, examining for the first time how each of the spectral components of the input light affect the self-healing characteristics. This study is also related to the original work of MacLeod showing a white focal line with Axicon focusing [11]. We explore this from both a numerical and experimental point of view. In particular we find that a white light Bessel beam self-heals into a spectrally disperse focal line that ultimately turns into a white focal line of light at a given distance beyond the obstacle. Towards the end of the propagation distance, the central spot will 'lose' its shorter wavelength components and retain only the longer wavelength spectral components. Therefore, the propagating white light Bessel beam can be divided into three regions: (1) a region where the chromatic aberration in the visible part makes the central spot of the Bessel beam transform colour from blue to purple, then to pink and finally to white, (2) a chromatic aberration free region where we have a true white light line and (3) a region where the chromatic aberration leads to a central spot which only contains the infrared part of the spectrum of the light source. Axicon generated white light focal lines [11] and white light Bessel beams have important consequences for enhanced axial focusing in optical coherence tomography [12] and optical micromanipulation [13], thus a detailed understanding of the spectral evolution of the generated and reconstructed beam is required for optimizing the source for a particular application.

In the next section we describe our generic experimental set up for white light Bessel beam formation and reformation beyond a symmetric opaque obstacle, followed by predictive calculations for the behaviour of the beam in the self-healing process which are subsequently verified by experiments.

2. Experiment

Bessel beams may be generated by both coherent and incoherent light sources, including halogen light bulbs, laser diodes below threshold and supercontinuum sources.

There are various different ways to generate Bessel beams, but here the method of beam generation using an Axicon was adopted due to the low losses associated with this scheme. In this case, the Gaussian input beam enters the conical lens (Axicon) on the flat side and leaves on the conical side (as shown in figure 2 for example), creating a conical wave. Hence, the k-vectors are arranged in cones, where the angle of each cone is defined by the wavelength. The superposition of the different k-vectors leads to an interference pattern
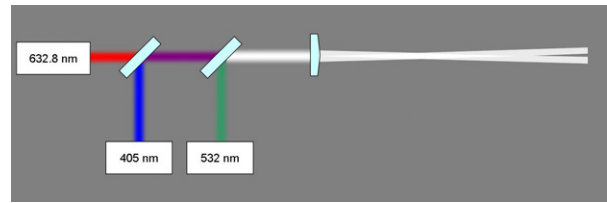
Figure 1. Experimental setup for the overlap of three different coloured laser beams with subsequent Bessel beam generation. The three lasers (helium–neon, $\lambda = 632.8$ nm; a violet laser diode, $\lambda = 405$ nm; and a green laser, $\lambda = 532$ nm) were overlapped using dichroic mirrors.
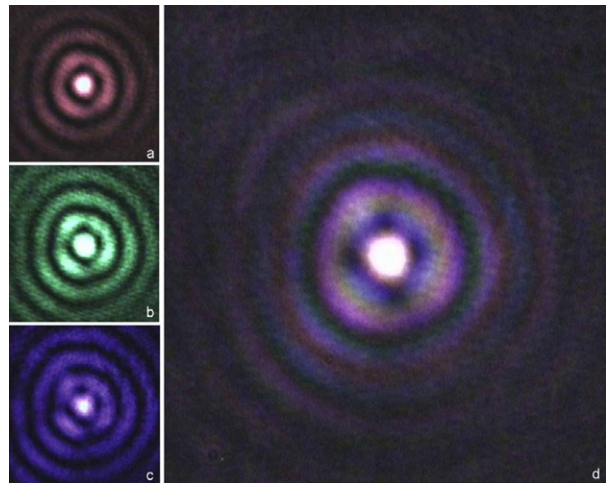

Figure 2. Superposition of three Bessel beams generated with different laser sources: (a) helium–neon ($\lambda = 632.8$ nm), (b) violet laser diode ($\lambda = 405$ nm) and (c) a green laser ($\lambda = 532$ nm, left bottom) to create a continuous wave white light line (right). The Axicon overlaps the three lasers (as shown in (d)) and creates a white light central spot notably compensated for the chromatic aberration, in contrast to the behaviour of a normal lens.

known as Bessel beam because the intensity distribution can be approximated by the square of the zero-order Bessel function.

In figure 1 we show how to generate a high power focal white line of light using three standard laser sources, namely a helium–neon laser (632.8 nm), a violet laser diode (405 nm) and a frequency doubled solid state laser (at 532 nm). The Axicon generates conical wavefronts for each wavelength, whereas in the centre they all overlap. This superposition creates a white light central spot, which is maintained over a long distance while propagating. Such a superposition is shown in figure 2 and we note the centre of the beam retains its white light nature, verifying the absence of chromatic aberration at the beam centre.

To study reconstruction, we carried out experiments using a supercontinuum light source with a spectrum ranging from 400 to 1100 nm, with a 400 nm full width half maximum (FWHM), centred at 500 nm. The supercontinuum was generated when pulses from a femtosecond Ti:sapphire (Femtosource, 10 fs, 80 MHz) laser propagated through a Femtowhite photonic crystal fibre (PCF), as shown in figure 3. We obtained up to 180 mW of supercontinuum light, which was then directed to an Axicon. The beam has a diameter of
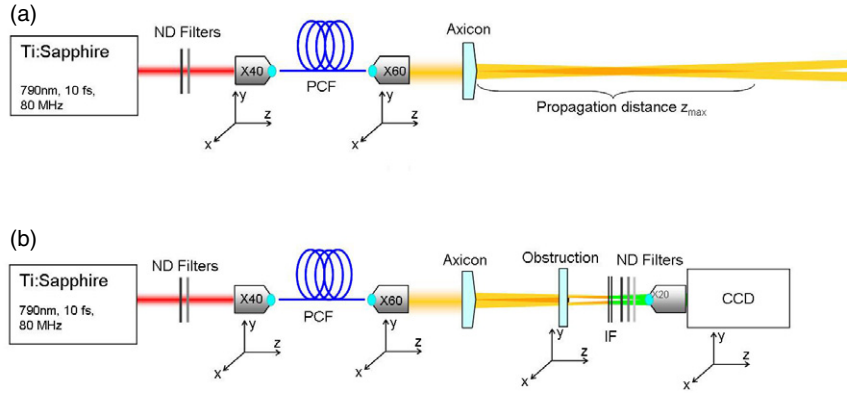
Figure 3. Experimental setup for (a) the generation of the Bessel beam and (b) for the measurement of the reconstruction distance z_{min}. The beam from a Ti:sapphire laser is coupled into a piece of a photonic crystal fibre (PCF). The different spectral components were obtained using interference filters (IF). The CCD camera is connected to a computer with image capturing hard- and software.
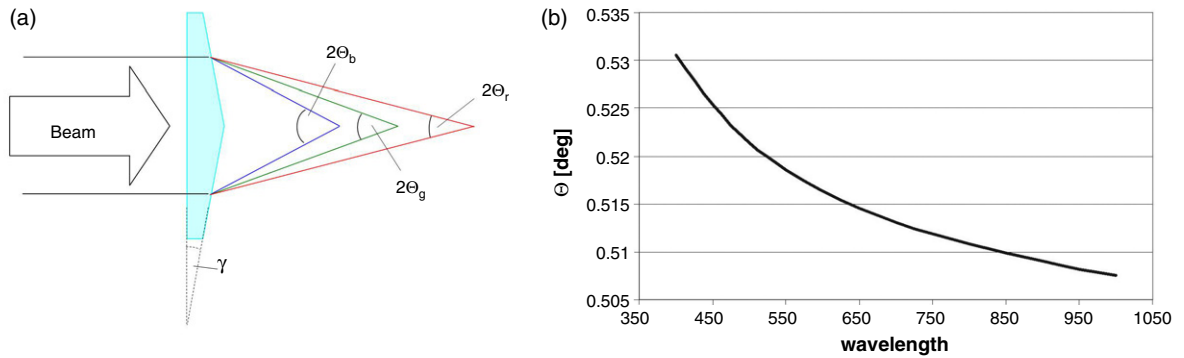

Figure 4. Wavelength dependency of the opening angle Θ of the radiation cone which is formed after the Axicon. (a) Schematic diagram of the rays of different spectral components after the Axicon and (b) calculation of Θ if $\gamma = 1°$.

about 2 mm on the input side of the Axicon, which leads to a typical propagation distance of the Bessel beam of about 12 cm (at a wavelength of 800 nm).

Figure 3(a) shows the setup for generation of the Bessel beam pattern and figure 3(b) displays the arrangement for the measurement of the reconstruction distances.

3. Calculations

We numerically calculated the behaviour expected when inserting an obstruction into the centre of the white light Bessel beam. We briefly summarize the results and focus on the description of the colours obtained in the generated Bessel beam pattern.

First, we note that the angle Θ which the k-vectors form after passing through the Axicon (with apex angle γ) is wavelength dependent (as shown in figure 4(a)) and given by

$$\Theta(\lambda) = (n(\lambda) - 1) \cdot \gamma. \tag{1}$$

This relation follows directly from Snell's law of refraction using the small angle approximation. The wavelength dependence of the angle Θ is due to the refractive index being a function of the wavelength, as displayed in figure 4(b).

From the wavelength dependence of the angle Θ (equation (1)), we can now derive a set of wavelength dependent parameters of broadband Bessel beams generated by an Axicon, including a wavelength dependent beam profile (which results in the coloured ring structure), a wavelength dependent propagation distance $z_{max}(\lambda)$ and also a wavelength dependent reconstruction distance $z_{min}(\lambda)$, as described in the following paragraphs.

3.1. Beam profile

The electrical field of a zero-order Bessel beam pattern generated at $z_{max}/2$ can be described by

$$E(r) \propto J_0(k_r \cdot r). \tag{2}$$

The radial intensity distribution is proportional to the squared electric field, thus proportional to the square of the zero-order Bessel function J_0. Using $k_r = k \cdot \sin(\Theta)$ and (1) the intensity reads

$$I(r, \lambda) \propto J_0^2(k \cdot \sin((n(\lambda) - 1)\gamma) \cdot r) \tag{3}$$

where J_0 is the zero-order Bessel function, k is the wave vector, $n(\lambda)$ is the refractive index, γ the apex angle of the Axicon and r the radius.

The calculated beam profiles are displayed in figure 5. The inset of figure 5 shows the Bessel beam generated from a supercontinuum light source.
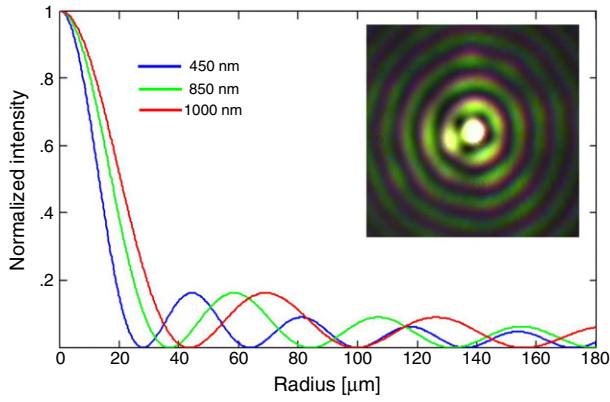
Figure 5. Calculated beam profiles of different spectral components of the Bessel beam generated from a supercontinuum, which is displayed in the inset on the top right side.
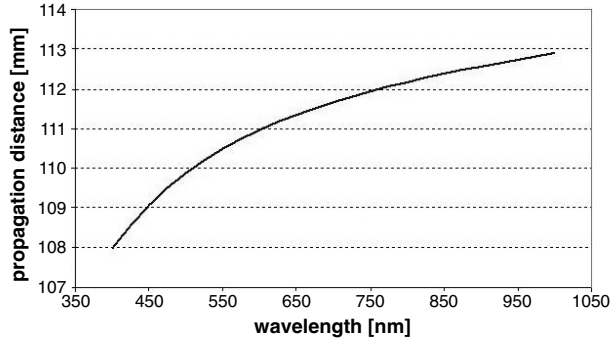

Figure 6. Propagation distances of the spectral components of a Bessel beam generated from a supercontinuum source (assuming $w_0 = 1$ mm).

3.2. Propagation

The propagation distance z_{max} of a Bessel beam is approximated by the ratio of the beam waist w_0 and the angle of the cone of the k vectors Θ. Using the relations mentioned above, the propagation distance can be written as

$$z_{max}(\lambda) \approx \frac{w_0}{(n(\lambda) - 1)\gamma}. \tag{4}$$

This relation is plotted in figure 6 for a BK7 Axicon with an apex angle of 178° (thus $\gamma = 1°$) and a beam waist of $w_0 = 1$ mm.

We make some general comments on this behaviour: typically one can distinguish the ring like structure of the Bessel light field, yet as can be seen in figure 5 the use of a very broad band light source with near equal weightings in each spectral component would lead to a washing out of the ring like structure yet retain the central maximum of the beam. In addition, we have a wavelength dependency of the propagation distance as expected, which means closer to the Axicon the shorter wavelength components dominate, whereas as we get further away from the Axicon the longer wavelength components dominate the spectral characteristics of the focal line.
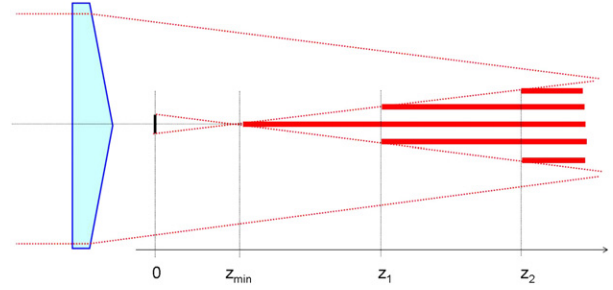
Figure 7. Reconstruction distances with respect to the number of reconstructed rings. For simplicity, only one wavelength is displayed. The obstacle is located at 0. After z_{min}, as given by formula (6), the central spot starts reconstructing. After z_1, the first ring and after z_2 the second ring has reconstructed.
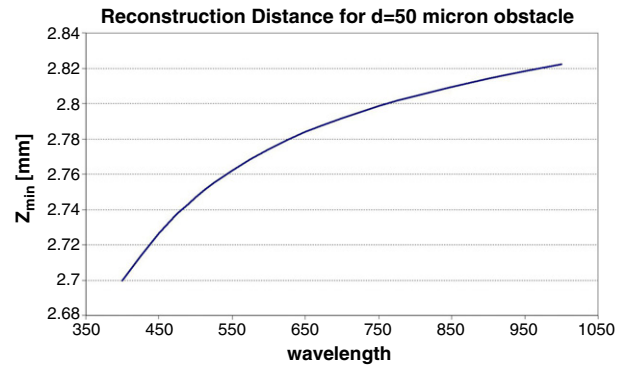

Figure 8. Calculated wavelength dependent reconstruction distances after a spherical obstruction with a 50 μm diameter. The Bessel beam is generated using an Axicon with an opening angle of 1°.

3.3. Reconstruction

The distance z_{min} after which a Bessel beam starts to reform when its central part is blocked by an opaque obstruction of radius r_{ob} is approximated using a simple geometrical approach.

$$z_{min} = r_{ob} \frac{k}{k_r} \tag{5}$$

which, for small apex angles γ can be approximated as

$$z_{min}(\lambda) \approx \frac{r_{ob}}{(n(\lambda) - 1)\gamma} \tag{6}$$

where r_{ob} is the radius of the obstruction, γ the apex angle and $n = n(\lambda)$ the refractive index of the Axicon, respectively. Note that z_{min} is the distance after which the central spot appears. As the beam further propagates, more and more rings reconstruct. Here, we define a new reconstruction distance which is a function of the Bessel beam radius r_{bb} as well.

$$z_{eff}(\lambda) \approx \frac{r_{ob} + r_{bb}}{(n(\lambda) - 1)\gamma}. \tag{7}$$

Here r_{bb} is the radius of the Bessel beam pattern which is reconstructed. This is illustrated in figure 7. After z_{min}, the central spot, after z_1, also the first ring and after z_2 also the second ring is reconstructed.

Figure 8 shows the calculated reconstruction distance, z_{min}, of the central spot when the beam is obstructed by an obstacle of 50 μm in diameter.
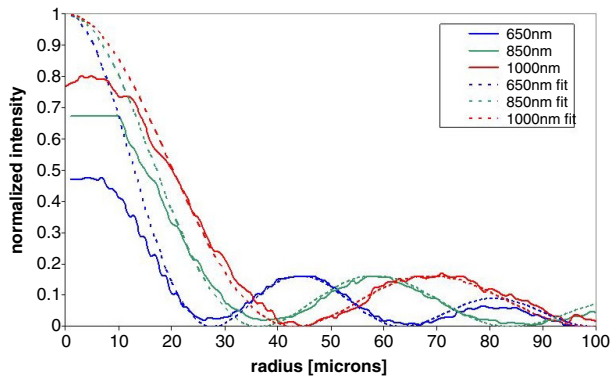
Figure 9. Measurement of the intensity profiles of different spectral components of a Bessel beam generated from a supercontinuum source. Measured values are displayed as solid curves whereas the calculated values are plotted as dashed curves. Note that the graph only displays the beam up to a radius of 100 μm; the beam extends much further after that. At small radii (near the axis) saturation of the camera means the experimental and theoretical fit deviate.
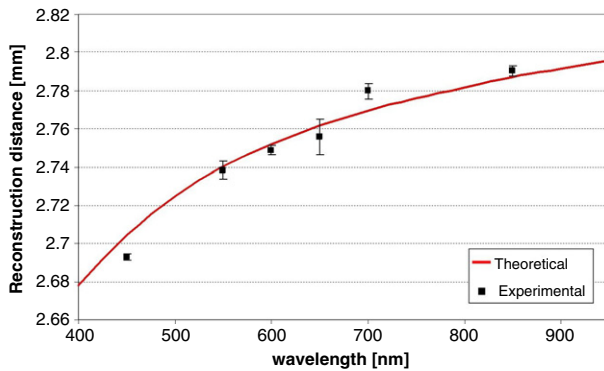

Figure 10. Experimental (points) and theoretical reconstruction distances of the central peak of the Bessel beam after being obstructed by an obstacle of 49.6($\pm$0.5) μm diameter. The experimental data points were obtained using interference filters. The points show the mean and the error bars show the standard error of the mean.

According to figure 2 we expect the shorter wavelength part of the spectrum to reform as a Bessel beam earlier than the longer wavelength part. Therefore, a blue central spot should be visible followed by a mixture of colours towards the white region as one moves along the axis behind the obstacle. This has indeed been experimentally observed, as displayed in figure 11.
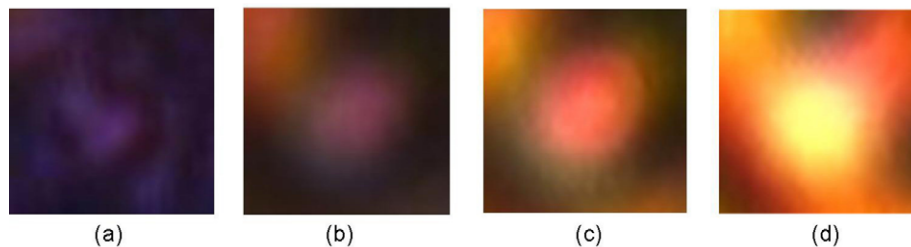
4. Results

4.1. Beam profiles

We inserted a circular symmetric obstacle of 49.6 μm diameter into the beam path of the generated Bessel beam. Beam profiles of the different spectral components were taken using a CCD camera at various distances beyond the obstruction. The spectral components were selected using interference filters. Note that the camera has a nonlinear response with respect to the different spectral components. The measured curves in figure 9 were normalized to the intensity of the first ring to compensate for the effect of the camera. To obtain the best line profiles the central spot was saturated, as can be seen in the radius range from 0 to 20 μm. The dashed lines in figure 9 show the squared zero-order Bessel function $J_0^2(k \sin((n(\lambda) - 1)\gamma)r)$ according to formula (3) with varying wavevector k and refractive index $n(\lambda)$ of the Axicon, as displayed in figure 5. As expected, the radial beam profiles of the different spectral components exactly follow the corresponding squared zero-order Bessel function.

4.2. Reconstruction

Figure 10 displays the measured distances after the obstacle at which the central spot is reconstructed after the beam has been obstructed by a circular obstacle. The obstacle diameter was measured along different axes by imaging on a camera using a microscope objective. The values obtained are in the range between 49 and 50 μm with an average of 49.6 $\pm$ 0.5 μm. The theoretical fit has been calculated by formula (6).

As expected, we observed a wavelength dependent reconstruction distance of the central spot. We observed the reformation of the spectral components to occur such that the shorter wavelengths reform first, at shorter distances from the obstacle. This yields a spectrally varying focal line in the Bessel beam, in contrast to what has been observed [11]. Note that after a distance of about 2.8 mm, all of the spectral components have reconstructed and we therefore have a 'white central peak'.

The Bessel beam generated from a white light source can thus, according to the presence or absence of chromatic aberration be divided into three different regions while propagating. (1) At the beginning, the chromatic aberration leads to a blue central spot, where while propagating more and more of the visible part of the spectrum comes in, leading to a white line. (2) This white line then propagates free of chromatic aberration over most of the propagation

Figure 11. Central spot of the supercontinuum generated Bessel beam. The colour changes from blue over purple and pink to white, as more and more spectral components have reformed.

distance z_{max}. (3) At the end of the propagation distance, the shorter wavelength part of the spectrum disappears in the central spot, leading to an infrared central spot with longer wavelengths dominant while propagating. These three sections are present in a white light Bessel beam with and without any obstruction—the obstruction however inserts an extra section (1), thus a region where the shorter wavelength part of the spectrum dominates.

The detailed knowledge of the spectral variation of a white light Bessel beam, particularly within the self-healing process is a prerequisite for advanced applications with such systems such as optical coherence tomography [12]. We additionally propose new studies using this geometry: a spectrally varying line such as this may have several uses: for example, imaging of cellular structures, cellular markers or fluorophores such as fluorescent proteins. These have different absorption and emission characteristics: by translating a spectrally disperse white light Bessel beam through a cell we would be able to excite multiple fluorophores sequentially in the cell. Indeed a detailed recording of the spectrally disperse central maximum in itself would act as an excellent signature of the properties of the illuminating white light source and its wavelength spread.

Acknowledgments

References

[1] Durnin J, Miceli J J and Eberly J H 1987 *Phys. Rev. Lett.* **58** 1499
[2] Arlt J, Dholakia K, Soneson J and Wright E M 2001 *Phys. Rev.* A **63** 063602J
[3] Garcés-Chávez V, McGloin D, Melville H, Sibbett W and Dholakia K 2000 *Nature* **419** 145
[4] Fan J, Parra E, Alexeev I, Kim K Y, Milchberg H M, Margolin L Ya and Pyatnitskii L N 2000 *Phys. Rev.* E **62** 7603
[5] Wulle T and Herminghaus S 1993 *Phys. Rev. Lett.* **70** 1401
[6] Fortin M, Piché M and Borra E F 2004 *Opt. Express* **12** 5887
[7] McGloin D and Dholakia K 2005 *Contemp. Phys.* **46** 15
[8] Fischer P, Brown C T A, Morris J E, Lopez-Mariscal C, Wright E M, Sibbett W and Dholakia K 2005 *Opt. Express* **13** 6657
[9] Basano L and Ottonello P 2005 *Am. J. Phys.* **73** 826
[10] Lin Y, Seka W, Eberly J H, Huang H and Brown D L 1992 *Appl. Opt.* **31** 2708
[11] McLeod J H 1960 *J. Opt. Soc. Am.* **50** 166
[12] Ding Z, Ren H, Zhao Y, Nelson J S and Chen Z 2002 *Opt. Lett.* **27** 243
[13] Little H, Brown C T A, Garces-Chavez V, Sibbett W and Dholakia K 2004 *Opt. Express* **12** 2560